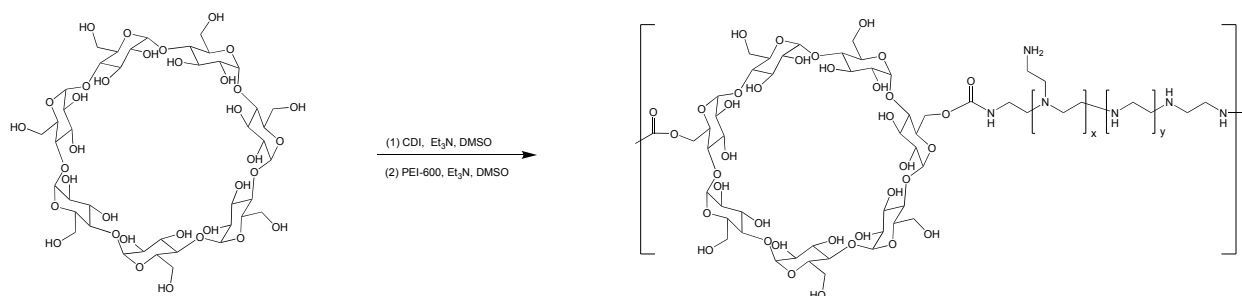


## A Zipped-Up Tunable Metal Coordinated Cationic Polymer for Nanomedicine

Jianming Mao<sup>a</sup>, Jianwei Wang<sup>a, b</sup>, Guping Tang<sup>a, b</sup>, Paul K. Chu<sup>b</sup>, Hongzhen Bai<sup>\*a, b</sup>

### Supplementary Figures and Discussions



**Scheme S1.** Synthetic procedures of PC. In the process, two hydroxyl groups of each  $\beta$ -cyclodextrin were activated and then conjugated by PEI (MW = 600).

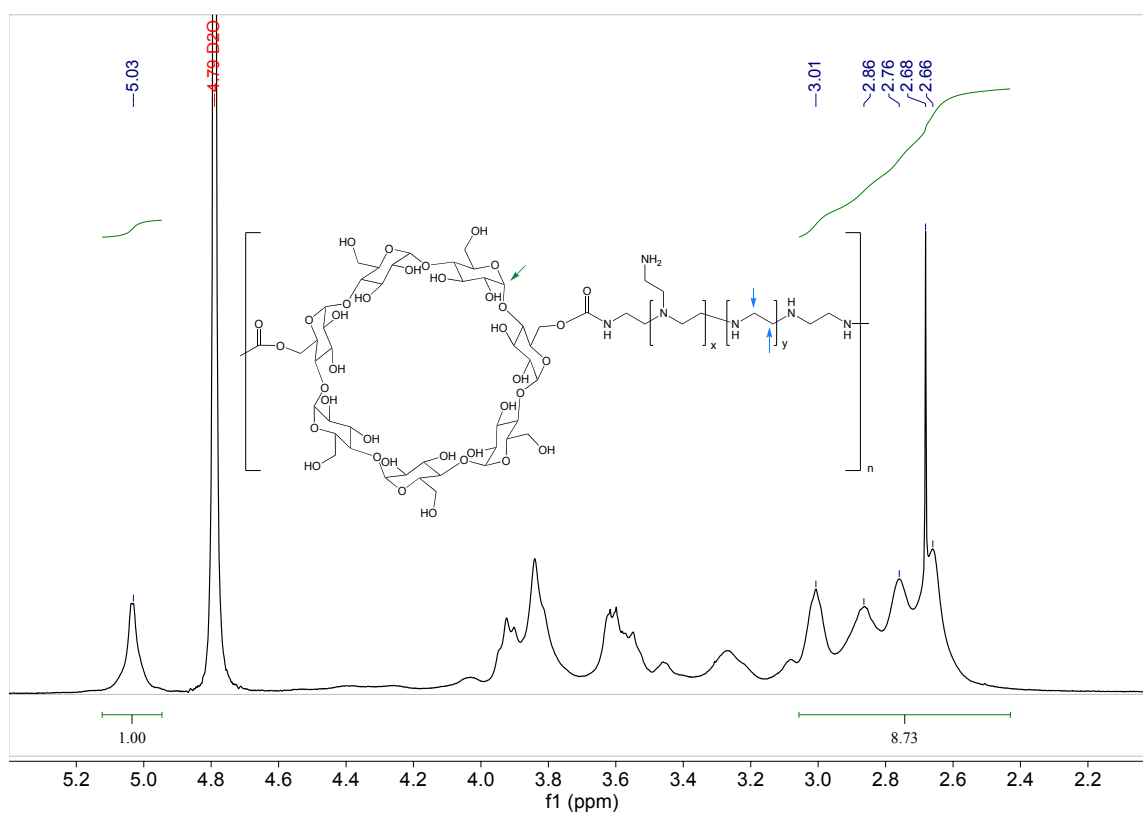


**Figure S1.** <sup>1</sup>H NMR spectrum of PC.

El.	Intensity (c/s)	Atomic %	Atomic Ratio	Conc	Units	Error 2-sig	MDL 3-sig
C	118.41	46.693	2.1004	31.976	wt.%	1.783	1.845
N	28.05	16.860	.7584	13.465	wt.%	1.776	2.088
O	96.96	22.230	1.0000	20.279	wt.%	1.114	.959
Cl	384.86	9.453	.4252	19.108	wt.%	.464	.245
Fe	75.69	4.765	.2143	15.171	wt.%	.859	.552
		100.000		100.000	wt.%		

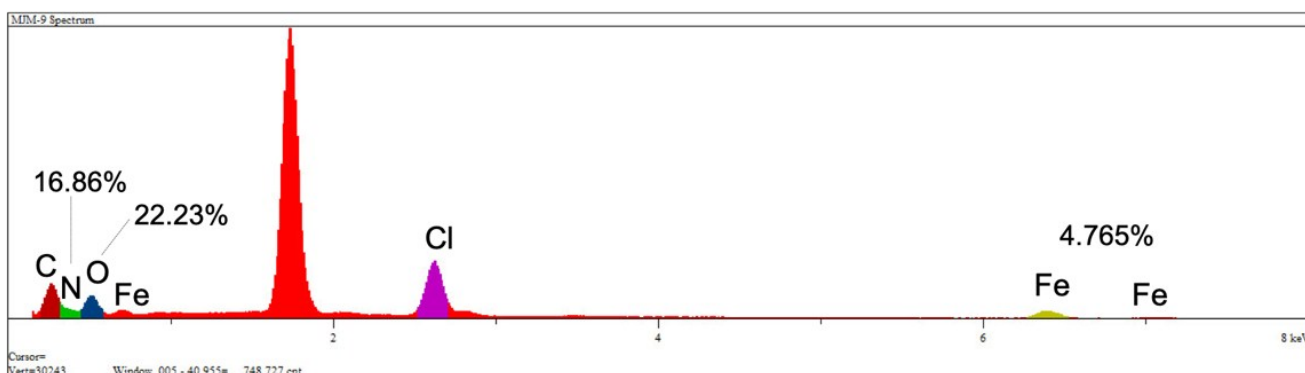


**Figure S2.** Elemental concentrations of MCCP with PC to Fe ratio of 1:1.

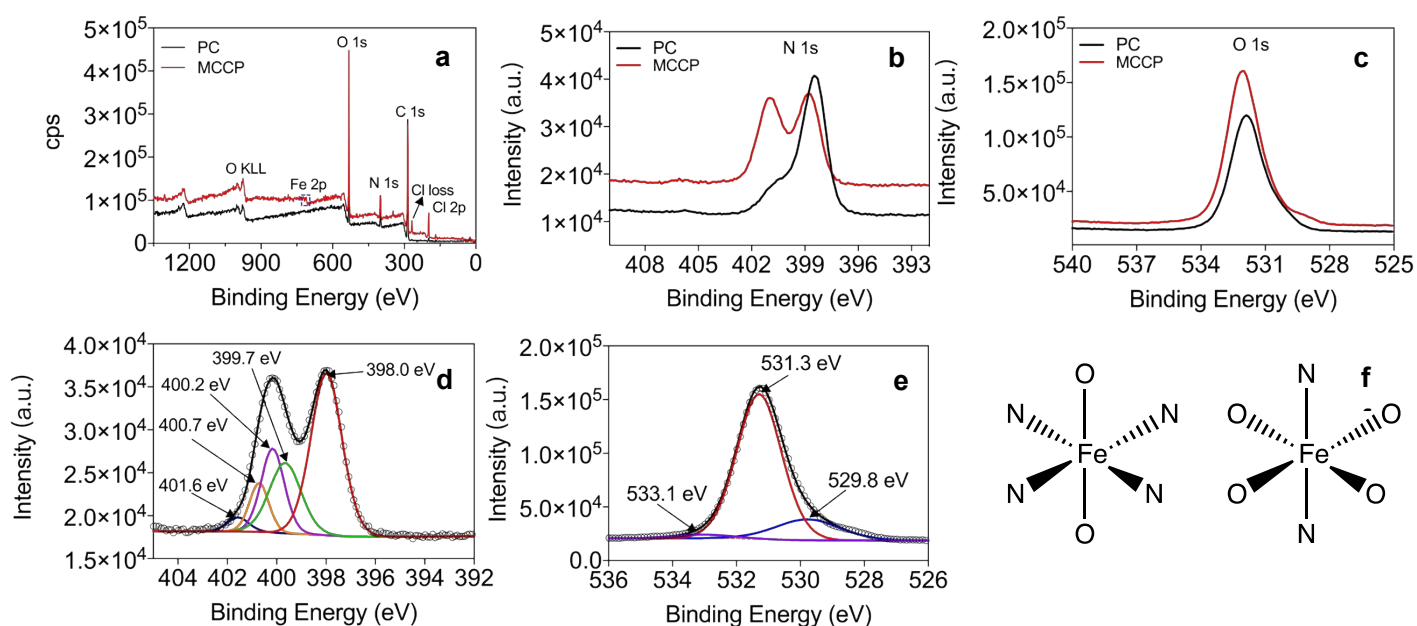


**Figure S3.** a) XPS survey spectrum of PC and MCCP. XPS b)  $N_{1s}$  and c)  $O_{1s}$  spectra and comparison of the chemical shifts of PC and MCCP indicating coordination of Fe-O and Fe-N. d) The  $N_{1s}$  XPS spectrum shows the peaks at binding energies of 398.0 eV, 399.7 eV, 400.2 eV, 400.7 eV, which are attributed to the C-N ( $1^\circ$ ), C-N-Fe, C-N ( $2^\circ$ ) and C-N ( $3^\circ$ ) bonds. e) The  $O_{1s}$  spectrum shows the peaks at binding energies of 529.8 eV, 531.3 eV and 533.1 eV, which are attributed to C-O-Fe, C-O and C-O(H)-Fe bonds. (f) Possible coordination between Fe and N, O.

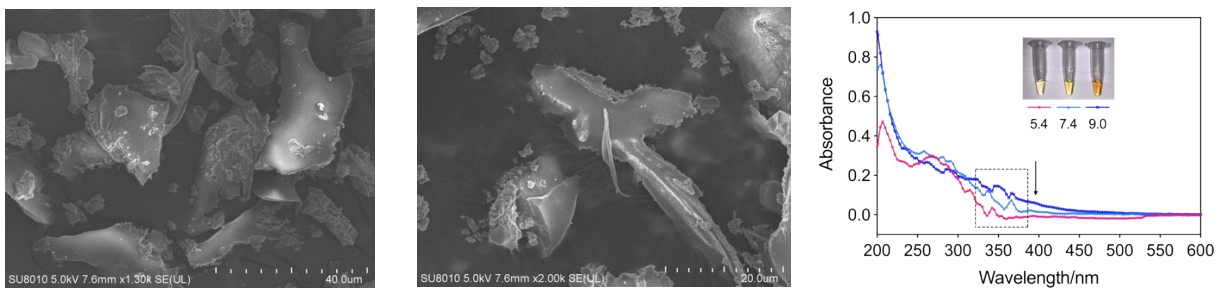


**Figure S4.** SEM images of MCCP prepared at pH = 5.4 (left and middle). UV-Vis spectra of MCCP prepared at different pH as indicated (right).

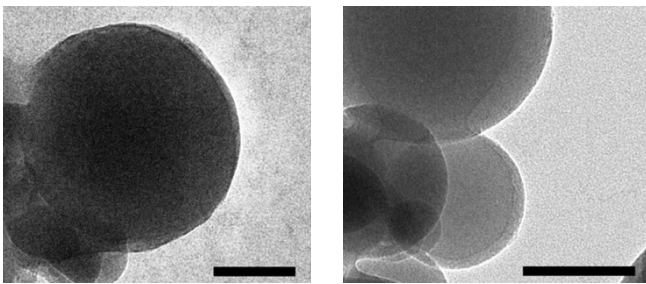


**Figure S5.** TEM images of SiO<sub>2</sub>@MCCP with PC:Fe ratios of 2:1 and 1:1 (scale bars = 100 nm).

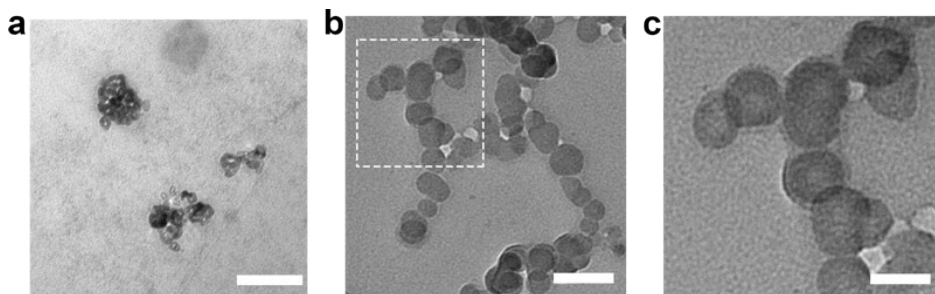


**Figure S6.** TEM images of (a) MCCP@TiO<sub>2</sub> (scale bar = 100nm), (b-c) MCCP@Sorafenib (scale bars = 100 nm and 50 nm)

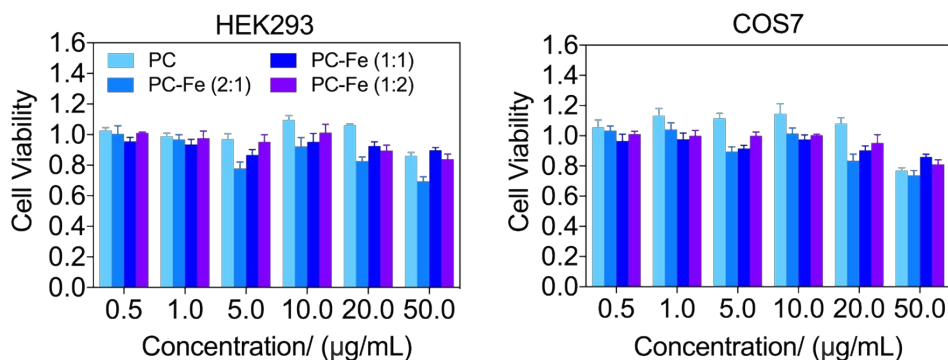


**Figure S7.** MTT assay of the HEK293 and COS7 cell lines treated with PC and MCCPs with different concentrations from 0.5 µg/mL to 50 µg/mL.

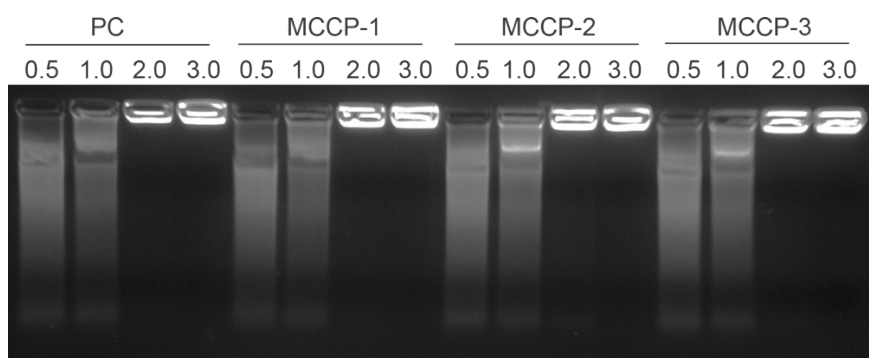


**Figure S8.** Gel retardation assays of MCCPs compared with PC.

**Table S1.** Size distributions and zeta potentials of DNA/MCCP and RNA/MCCP in comparison with those of DNA/PC and RNA/PC.

Nucleic Acid	Material	Average Size (nm)	Average Zeta potential (mV)
DNA	PC	111.9 ± 48.68	30.0 ± 5.1
	MCCP-1	160.9 ± 82.34	22.7 ± 7.9
	MCCP-2	159.5 ± 66.84	17.1 ± 8.3
	MCCP-3	184.8 ± 99.06	13.9 ± 4.8
RNA	PC	154.8 ± 53.56	35.0 ± 6.9
	MCCP-1	221.2 ± 153.3	29.7 ± 7.3
	MCCP-2	28.99 ± 7.19	28.7 ± 7.09
	MCCP-3	361.9 ± 158.9	
	MCCP-3	154.1 ± 80.43	16.0 ± 6.0
		629.4 ± 265.4	

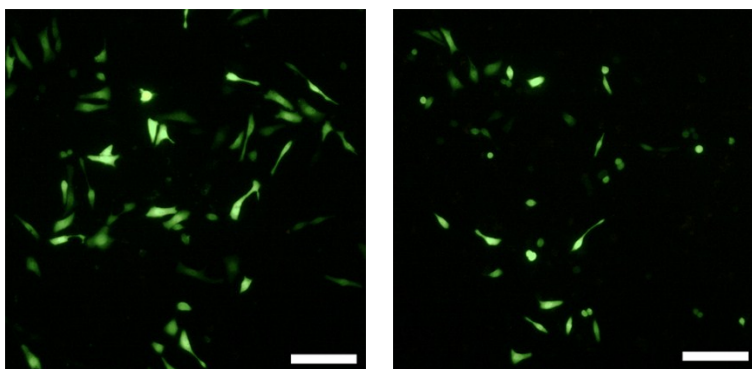


**Figure S9.** Fluorescence image of HEK 293 cell line treated with (left) pEGFP/PC and (right) pEGFP/MCCP-2 (scale bars = 100  $\mu$ m).

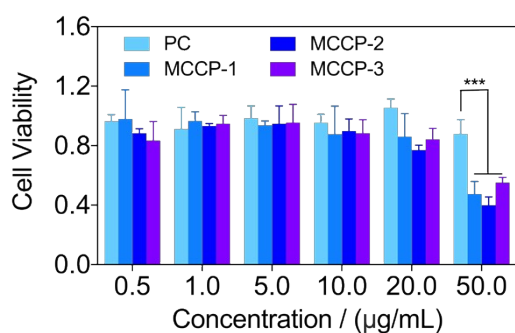


**Figure S10.** MTT assay of PC and MCCPs in KB cancer cells. When the concentration was increased to 50  $\mu$ g/mL, significant cell death was observed compared to cells treated with PC (data represent mean  $\pm$  SD, n = 3; \*\*\*, P < 0.001).

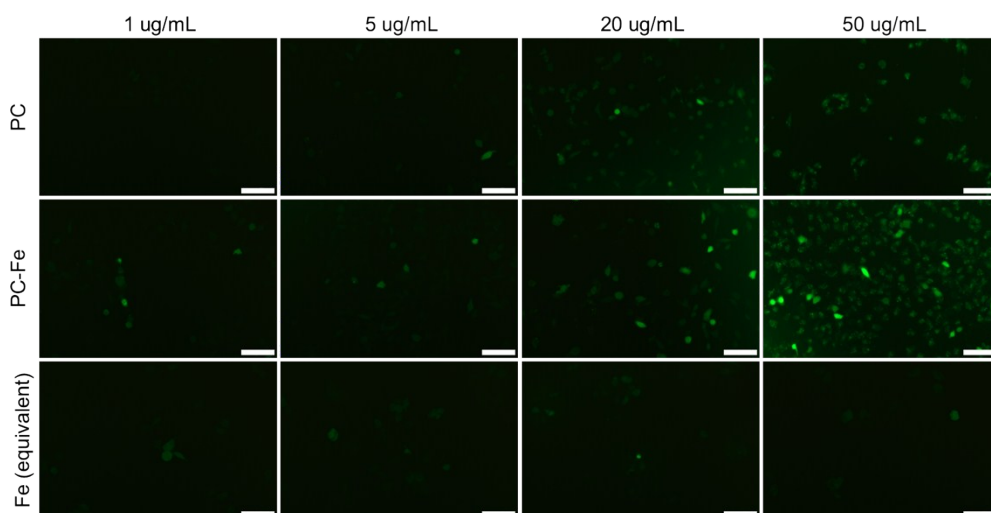


**Figure S11.** DCF fluorescence from KB cells treated with PC, MCCP-2 and equivalent Fe<sup>III</sup> solutions (scale bar = 100  $\mu$ m)

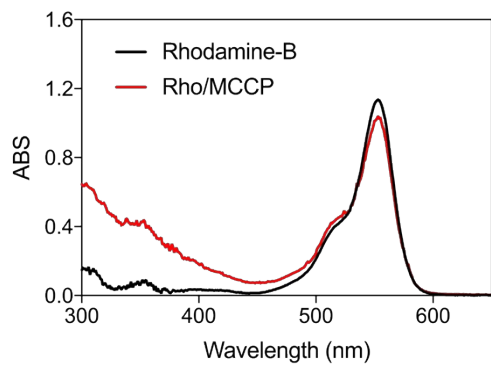


**Figure S12.** UV-Vis spectra of Rhodamine-B and Rho@MCCP.